PCCP

PAPER

View Article Online
View Journal | View Issue



Cite this: *Phys. Chem. Chem. Phys.*, 2025, **27**, 16951

# Linear superposition behavior of blended salt organic carbonate-based electrolyte formulations†

Nico Spreckelmeyer,[a] Peng Yan,[b] Moumita Maiti,[a] Anand Narayanan Krishnamoorthy,[b] Christian Wölke,[b] Isidora Cekic-Laskovic,[b] Martin Winter,[b] Diddo Diddens[b] and Andreas Heuer*[a]

The design of an electrolyte to improve the performance of the resulting battery chemistry depends on many factors. Greater variability is achieved by using a mixture of conducting salts rather than a single salt. Experimentally, the ionic conductivity for different anion pairs is shown to change linearly as one electrolyte component is gradually replaced by the other. Using molecular dynamics simulations with a polarizable force field, the change in structural and transport properties is analyzed and discussed for the specific case of lithium hexafluorophosphate ($LiPF_6$) and lithium bis(fluorosulfonyl)imide (LiFSI). In addition to a quantitative reproduction of the experimental ionic conductivities, insight into the dependence of the microscopic mechanisms on the conductivity upon salt substitution is presented by comparing the blended salt electrolyte with the same number of anions with the two limiting single salt electrolytes. It is found that the structure of the blended salt electrolyte, as characterized by lithium nearest neighbor shells, can be well predicted from the structure of the two single salt electrolytes under the assumption of random mixing. Furthermore, the structural and dynamical properties of the lithium anion pairs are basically insensitive to the salt composition, *i.e.* they exhibit mixing invariance. It is argued that the validity of random mixing and mixing invariance, together with the hydrodynamic effects of cross correlations between like ions, justify the linear composition dependence of the conductivity. Additionally, distinct differences are identified in how lithium interacts with either $PF_6^-$ or $FSI^-$ anions.

Received 13th February 2025,
Accepted 21st July 2025

DOI: 10.1039/d5cp00588d

rsc.li/pccp



## 1 Introduction

The performance of a battery is contingent upon the bulk properties of the electrolytes and the electrode|electrolyte interface. Consequently, the design of both electrolyte and electrode compositions is crucial. It is evident that no single electrolyte formulation can provide optimal bulk and interface properties, which presents a considerable challenge to the design of an optimal electrolyte. Electrolytes can exist in either a liquid or solid state. Generally, liquid electrolytes display higher ionic conductivities as solid electrolytes. Among the liquid electrolytes that have been used in commercial Li ion batteries for a long time are organic carbonate-based electrolytes, as evidenced by citations.[1–3] One of the challenges in the design of Li ion batteries is to select an appropriate anion for the conducting salt. Lithium hexafluorophosphate ($LiPF_6$) is currently the most widely used conducting salt in commercial batteries[4,5] due to its relatively high ionic conductivities of resulting electrolyte formulations as well as its beneficial impact on interphase formation. Furthermore, $LiPF_6$ can protect the Al current collector by forming $AlF_3$ and thus preventing Al dissolution.[6] Many other conducting salts have advantages over $LiPF_6$ by providing higher ionic conductivity, a wider electrochemical stability window and functionality over a wider temperature range *etc*, but at the same time there are disadvantages. Properties such as ionic conductivity and thermal stability are less optimised with $LiPF_6$ than with lithium bis(fluorosulfonyl)imide (LiFSI)[7] in organic carbonate electrolytes. The main disadvantage of LiFSI is that it dissolutes aluminium under typical battery operating conditions. On the other hand, lithium tetrafluoroborate ($LiBF_4$) has a lower ionic conductivity than $LiPF_6$ in organic carbonate electrolytes, but is a promising candidate for high voltage batteries.[8] Lithium bis(oxalato)borate (LiBOB) is another promising candidate which has a wider window of electrochemical and thermal

[a] *Institute of Physical Chemistry, University of Münster, Corrensstraße 28/30, 48149 Münster, Germany. E-mail: andheuer@uni-muenster.de*
[b] *Forschungszentrum Jülich GmbH, Helmholtz-Institute Münster (IMD-4), Corrensstraße 48, 48149 Münster, Germany*

† Electronic supplementary information (ESI) available. See DOI: https://doi.org/10.1039/d5cp00588d

stability,[9] it also forms an effective protective layer with Al to protect against corrosion.[10] However, it has the disadvantage of a lower ionic conductivity than $LiPF_6$.[11] Therefore, there is no single conducting salt that can meet all the performance requirements of a battery.

There are many attempts to identify novel and optimize existing electrolyte formulations, but it is extremely challenging because it requires the exploration of the large chemical space. The machine learning approach[12] makes this attempt somewhat easier, but still challenging as the application of machine learning is only recently initiated.

One approach is to combine the properties of different readily available conducting salts on a molecular level. To improve, *e.g.*, the properties of both LiBOB and $LiBF_4$ one can choose a chemical structure comprising the half molecular moieties of LiBOB and $LiBF_4$, which is lithium difluorooxalate borate (LiDFOB).[13] It turns out that the temperature dependence of the ionic conductivity of LiDFOB is always close to the component with the higher ionic conductivity (at high temperatures: LiBOB, at low temperatures: $LiBF_4$) and many other advantages are reported as well.[13] Another promising approach, which is the topic of this work, is the use of mixtures of available conducting salts.[14] For example, the 1 : 1 $LiBF_4$ and $LiPF_6$ blended salt electrolyte has a better high voltage performance than the respective single salt electrolyte formulations.[15] A conducting salt in a salt blend can even act as an additive to improve some aspects of battery performance.[16] Furthermore, the galvonostatic cycling performance is improved by the additional use of LiDFOB, lithium difluorophosphate (LiDFP), and lithium difluoro(bisoxalato)phosphate (LiDFBP)[17] whereas for LiDFP also the electrochemical performance is improved at low temperature.[18]

Beyond a detailed experimental characterization of macroscopic effects, a microscopic characterization and resulting identification of, *e.g.*, structure–performance relations is of utmost interest as well. Here, computer simulations can provide information about microscopic aspects of the system such as the local structure and connect it to macroscopic properties such as the ionic conductivity. In principle this knowledge may even help in the design of novel electrolytes.[19] Various simulation methods are available. The high accuracy of quantum mechanical *ab initio* studies is offset by a high computational effort. To perform efficient classical MD simulations with quantum–mechanical accuracy, machine learning approaches have recently become broadly accessible. However, application to blended salt electrolytes is still a challenge.[20,21] Here we use empirical potentials to simulate electrolytes. Whereas the non-polarisable OPLS-AA force field underestimates the transport behavior, incorporation of polarisation effects[22,23] allows for excellent agreement of structural and transport properties with the experiment. This has recently been shown in our work for the example of organic carbonate-based electrolytes.[24]

Here we analyse the mixing properties of LiFSI and $LiPF_6$ electrolytes. Experimentally, we observe a surprising linear dependence of the ionic conductivity on the composition, which is also present if LiFSI is replaced by LiBOB or $LiBF_4$, respectively. To gain a more detailed microscopic understanding of the two single salt and mixed electrolyte formulations, the structural and dynamic behaviour is studied in detail using MD simulations. Very good agreement of the ionic conductivities with the experimental values are observed. We introduce two criteria to characterize the mixing properties. First, we check to which degree the structural and dynamical properties of the lithium and anions, as well as the pair properties, remain identical after mixing. Insensitivity upon mixing is denoted mixing invariance. For this purpose, we also apply a newly developed method to characterize the dynamic correlation between lithium and anion motion.[25] Implications for the respective Onsager coefficients and the resulting conductivity are discussed. Second, we check whether in the blended salt electrolyte the anions are randomly distributed in the sample, *i.e.* display random mixing. Altogether, this analysis provides microscopic insight into the observed linear dependence of ionic conductivity on salt composition and allows to characterize the relationship between structural and dynamical effects.

# 2 Methods

## 2.1 Simulations

The MD simulation is performed with the simulation code Lucretius, developed at the University of Utah, using the APPLE&P force field parameters[22] at constant number of atoms, constant pressure 1 atm and constant temperature 333 K, if not mentioned otherwise. The force field differs from the OPLS-AA mainly due to the interaction between induced point dipoles and the electric field resulting from partial charges and other dipoles. The system is equilibrated for 4 ns followed by a subsequent production run of 100 ns. Both temperature and pressure are maintained using the Nosé–Hoover chain thermostat (coupling frequency 0.01 $fs^{-1}$) and barostat (coupling frequency 0.0005 $fs^{-1}$). Electrostatic interactions have been treated by the Ewald summation technique with a cut-off radius of 12 Å, an inverse Gaussian charge width of 0.23 $Å^{-1}$, and $7 \times 7 \times 7$ vectors for the reciprocal space. Lennard-Jones interactions have been truncated at 12 Å, beyond which a continuum model dispersion correction is applied. All bonds are constrained by the SHAKE algorithm.[26] A multi time-step integration scheme is implemented to integrate the equation of motion, see ref. 27 and 28 for more details. A time step of 0.5 fs is used for bonds and angles, respectively, while 1.5 fs is used for torsions and non-bonded interactions up to a distance of 7 Å. Finally, for non-bonded interactions above 7 Å a time step of 3 fs is used, and the same time step is also used for the reciprocal part of the Ewald summation.

We choose systems containing $LiPF_6$ and LiFSI as conducting salts and ethylene carbonate (EC) and ethyl methyl carbonate (EMC) as solvent/co-solvent. The molar salt concentration for the two single salt electrolytes as well as the blended salt electrolytes, concentrating on a mixing ratio of 50 : 50, is always 0.95 M. The weight ratio of EC and EMC is chosen to be 24 : 76 which is close to the typical weight ratios used in experiments.

 

The respective numbers of solvent molecules used in the simulations were 149 and 400, respectively. As a comparison we also performed simulations with a molar salt concentration of 2 M.

### 2.2 Ionic conductivity

The ionic conductivity is determined from simulations *via* eqn (1), where $N$, $z_i$, $V$ and $\Delta t$ are total number of ions, charge of an ion $i$, the box volume, and the duration for which the displacement $\Delta r_i$ is calculated. $\alpha$ and $\beta$ are indices either for cation or anion. It has self and cross correlations of the ions, the first term is the self correlation and the second and third terms are the cross correlations. The diffusivity $D$ can be obtained from the self-correlation, and the ionic conductivity resulting from the self-correlation alone corresponds to the Nernst–Einstein (N–E) conductivity $\sigma_{NE}$.

The overall ionic conductivity can be written as

$$\sigma = \lim_{\Delta t\to\infty} \frac{e^2}{6Vk_B T\Delta t} \sum_{i=1}^{N}\sum_{j=1}^{N} \langle z_i z_j \Delta r_i(\Delta t)\Delta r_j(\Delta t)\rangle$$

$$= \lim_{\Delta t\to\infty} \frac{e^2}{6Vk_B T\Delta t} \left( \sum_{\substack{i\\ i=j;}}^{N}\sum_{j}^{N} \langle \Delta r_i(\Delta t)\Delta r_i(\Delta t)\rangle \right.$$

$$+ \sum_{\substack{i\\ i\neq j; z_i=z_j}}^{N}\sum_{j}^{N} \langle \Delta r_i(\Delta t)\Delta r_j(\Delta t)\rangle$$

$$\left. -2\sum_{\substack{i\\ i\neq j; z_i\neq z_j}}^{N}\sum_{j}^{N} \langle \Delta r_i(\Delta t)\Delta r_j(\Delta t)\rangle \right)$$

$$\equiv \sigma_{NE} + \sigma_{++} + \sigma_{--} - 2\sigma_{+-} \quad (1)$$

$$\equiv \sigma_{NE}\left[1 + \frac{\sigma_{++}}{\sigma_{NE}} + \frac{\sigma_{--}}{\sigma_{NE}} - 2\frac{\sigma_{+-}}{\sigma_{NE}}\right]. \quad (2)$$

The term $2\sigma_{+-}$, reflects the interaction among distinct ions with unlike charges whereas the terms $\sigma_{++}$ and $\sigma_{--}$ express the distinct correlation of like charges, excluding the single-particle terms, contributing to $\sigma_{NE}$. The correction of Nernst–Einstein conductivity can be conveniently expressed by dimensionless values $\frac{\sigma_{ij}}{\sigma_{NE}}$.

### 2.3 Coupling of contact ion pairs

When studying the dynamic behavior of contact ion pairs, *i.e.* nearby lithium anion pairs, it is expected that due to the attractive interaction there exists a positive correlation between the motion of both entities until in the long-time limit they disengage and become uncorrelated. To study this scenario in more detail, in recent work[25] a numerical formalism has been introduced which allows one to characterize dynamic correlations in detail (Fig. 1).

At the initial time $t_0$ (over which we average) all contact ion pairs are identified. Then for each ion $i$ the displacement $u_i$ until the time $t_0 + t$ is determined. Furthermore, the displacement vector of any anion $j(i)$, forming a contact ion pair with ion $i$, is taken and projected on the displacement vector of the ion $i$. The length of this projected vector is denoted $v_{\parallel,j(i)}$. Furthermore, we define $\Delta v_{\parallel,j(i)} = v_{\parallel,j} - u_i$. When plotting the distribution of $\Delta v_{\parallel}$ for the chosen time $t$ important information about the nature of the correlated dynamics of cations and anions can be gained.

To capture the information content of this distribution by a single number one can define the coupling constant

$$\lambda(t) = \frac{\langle \vec{u}_i \cdot \vec{v}_i\rangle_t}{\langle \vec{u}_i^2\rangle_t}. \quad (3)$$

where the numerator and denominator are averaged over all lithium ions and its neighboring anions. If all contact ion pairs display an identical displacement, *i.e.* are translated as a rigid entity, one has $\lambda = 1$. In the other extreme of uncorrelated dynamics one obtains $\lambda = 0$.

### 2.4 Experiments

The conductivity cells were filled in a glovebox and the experiments were conducted under inert atmosphere (MBraun, $H_2O$ and $O_2 < 1$ ppm) *t*. Conductivity cells were filled with the various electrolyte formulations as previously described.[30] Cell constants were calibrated using a 0.01 M solution of KCl in $H_2O$ at 293 K (VWR, with a known ionic conductivity of 1.276 mS cm$^{-1}$) and determined by averaging five measurements. Impedance measurements were conducted using a Metrohm Autolab/M204

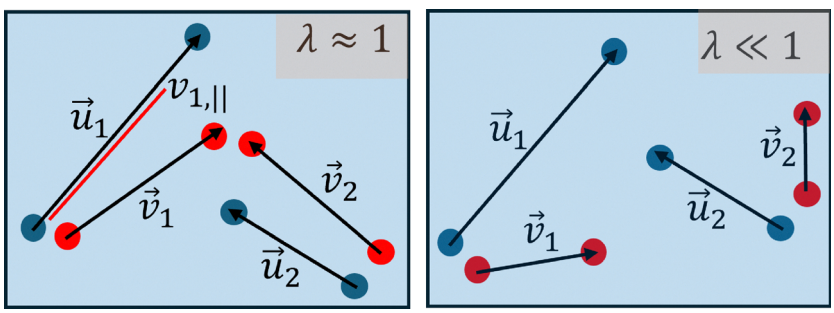


Fig. 1 Sketch to rationalize high and low values of the coupling constant $\lambda(t)$. Basically for $\lambda \approx 1$ one observes a highly correlated motion of the lithium ion (here: $\vec{u}_i$) and anions in its first neighbor shell (here: $\vec{v}_i$) during a fixed time $t$. For the formal definition, see text.

potentiostat/galvanostat in the frequency range of 50–20.000 Hz using in-house developed electrodes. The ionic conductivity of the considered electrolytes was determined in the temperature range from 243 K to 333 K in steps of 10 °C in a Memmert TTC256 temperature chamber, with each temperature held for 2 h prior to the measurement for equilibration. Impedance spectra were analyzed using the Metrohm Nova software and fitted with a model incorporating parameters for resistors $R_s$ and $R_p$, along with a constant phase element (CPE). The fitting procedure was updated at each new data point using the $R_s$ (CPE – $R_p$) model. Electrolyte conductivity values were obtained from the ratio of the cell constant and the determined electrolyte resistance. The shown experimental data are part of a larger data set obtained from high-throughput screening (HTS) experiments.

Viscosity and density measurements were conducted using an Anton Paar SVM 3001 viscometer. These measurements were carried out at a temperature of 333 K. To prevent contamination between tests, the instrument was cleaned with acetone after each measurement.

# 3 Results

For the results, we focus on key electrolyte properties, characterizing the structure and the ionic transport, including correlations among the ions and time scales of cation–anion pairing. In all cases, we analyze how the specific properties change when comparing the limiting cases of single salt electrolytes with the blended salt electrolyte formulations.

## 3.1 Structure

To elucidate the structural properties, the radial distribution functions (RDFs) of the $PF_6$/FSI anions around a Li ion are calculated, where the molecules are represented by their centre of mass. For both blended salt and single salt electrolyte formulations, the RDFs are shown in Fig. 2(a) and (b). Obviously, the interaction of Li with the $PF_6^-$ anion is significantly stronger than with the $FSI^-$ anion. Furthermore, the distance-dependence, obtained either for the single salt or blended salt electrolyte, look very similar. Closer inspection shows that the nearest-neighbor peak of Li–$PF_6$ is slightly increased for the blended salt electrolyte as compared to the single salt electrolyte whereas the opposite behavior is observed for Li–FSI. This likely reflects that due to the stronger Li–$PF_6$ interaction in the blended salt electrolyte some extra Li–$PF_6$ pairs are formed at the expense of Li–FSI pairs to further lower the free energy of the system. Apart from these small deviations the results are compatible with the random mixing scenario because of similar amplitudes and structural mixing invariance because of identical distance dependence of the RDFs.

Similarly to the oppositely charged ion pairs, the anion–anion pairs in the mixed salt have the same RDFs as in the single salt electrolyte formulations, see Fig. 2(c) and (d), also supporting the random mixing scenario and the structural mixing invariance for the anionic structure. To a large extent, the stronger effective attraction of $PF_6^-$ pairs may be a consequence of the strong Li–$PF_6$ interaction, so that lithium ions can act as a glue when two $PF_6$ anions are nearby. Interestingly, the RDF between FSI and $PF_6$ shows that their interaction is similarly weak compared to FSI pairs, see Fig. 2(e). This is consistent with the interpretation that only the specific interaction between lithium and $PF_6$ is strong, so that in contrast to $PF_6$–$PF_6$ pairs no effective attraction between FSI and $PF_6$ can be induced by nearby lithium ions. Furthermore, we would like to stress that the similarity of the FSI–FSI and FSI–$PF_6$ RDFs allows one to conclude on a qualitative level that there is no significant phase separation into $FSI^-$ and $PF_6^-$ rich domains.

To confirm that the preference of the $LiPF_6$ interaction is not an artifact of the force field, we have performed DFT-simulations of appropriately chosen small clusters, following the approach from ref. 29. As outlined in detail in the ESI,† the same tendency could be found with different DFT functionals. Additionally we checked whether the conclusions change if the anions are characterized by individual atoms (P for $PF_6$ and N for FSI). The resulting RDFs, as shown in the ESI,† fully support the picture, discussed above.

For a closer analysis of the degree of random mixing we characterize the first solvation shell of a Li ion with a three-digit number, where the first digit denotes the number of anions and the other two digits express the number of EC and EMC molecules, respectively. The radius of the shell is determined by the first minimum of the RDF, chosen to be 4.3 Å. This distance is close to the minimum of the Li-EC and Li-EMC RDF, respectively, as shown in ref. 24. The selected lithium anion pairs can be identified as contact ion pairs. The probability of appearance is defined as the ratio of the number of shells and the total number of Li ions. For the data, shown in Fig. 3(a), we do not distinguish between the $FSI^-$ and $PF_6^-$ anions. Beyond the probabilities for the blended salt electrolyte, we also display the average of the two single salt systems for each shell. It turns out that the distributions for both blended salt and single salt electrolytes are remarkably similar over the whole range of relevant Li ion shells.

To characterize the residual differences and find a direct relation to the observations from the RDF, we next keep track of the anion identity and compare the lithium shells with at least one anion. We start with the shell with one anion such as 112. For a direct comparison of the blended salt and single salt electrolytes, we need to reduce the probabilities of the single salt electrolytes by a factor of 2 due to the dilution of the respective anions. A reasonable agreement can be found for the predicted and the actual probabilites in the blended salt electrolytes, see Fig. 3(b) and (c). Furthermore, the outcome of the analysis of the RDF is recovered, namely the much stronger Li–$PF_6$ interaction as compared to the Li–FSI interaction. Also, a small increase (decrease) is seen in the number of Li–$PF_6$ (Li–FSI) pairs, which was already expected from the properties of the RDFs (and discussed there). This constitutes a minor correction to perfect random mixing.

The results from Fig. 3, discussed so far, are also compatible with the scenario that the blended salt electrolyte is somewhat separated in $PF_6^-$ and $FSI^-$ rich regions, which would

 

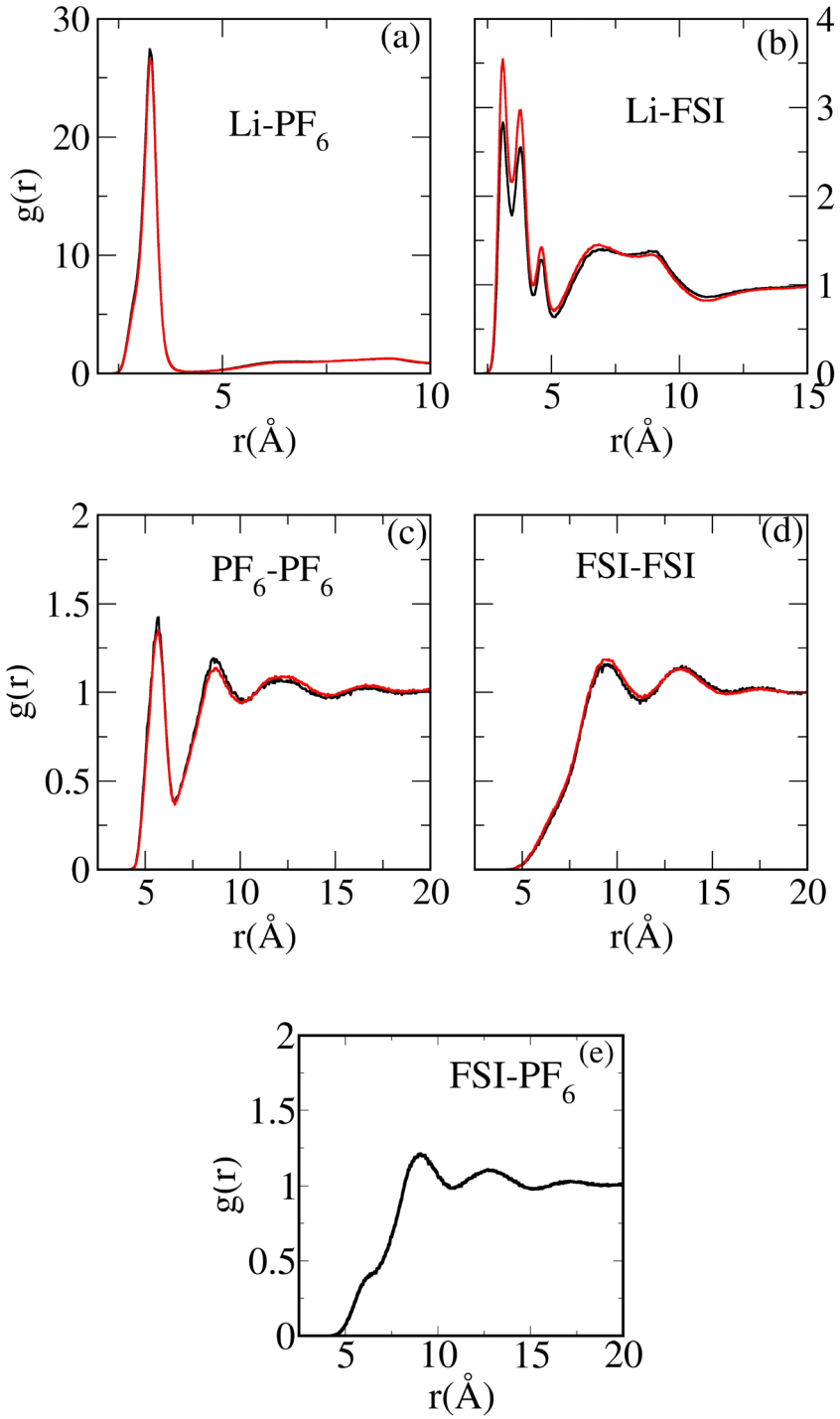


Fig. 2 Radial distribution function of (a) Li–$PF_6$ pairs, (b) Li–FSI pairs, (c) $PF_6$–$PF_6$ pairs, (d) FSI–FSI pairs, and (e) FSI–$PF_6$ pairs in blended salt electrolyte (black) is compared with respective single salt conducting salts (red).

invalidate random mixing. Whereas qualitative conclusions have already been drawn from the FSI–$PF_6$ RDF, the analysis of the 202 shell in Fig. 3(b), involving the binding of lithium to two $PF_6$ anions, allows more quantitative conclusions. Its (small) probability is proportional to the square of the ratio of $PF_6$ anions and accessible lithium cations. In case of strict random mixing this ratio decreases by a factor of 2 whereas in the extreme limit of strict phase separation this ratio remains constant. Thus, when comparing the 202 probability in the single salt $LiPF_6$ electrolyte to the probability in the blended salt electrolyte, the total reduction factors read 4 and 2, respectively. In Fig. 3(b) it is shown that with a reduction factor of 4 a very good agreement is reached. This strongly supports the random mixing scenario in the blended salt electrolyte.

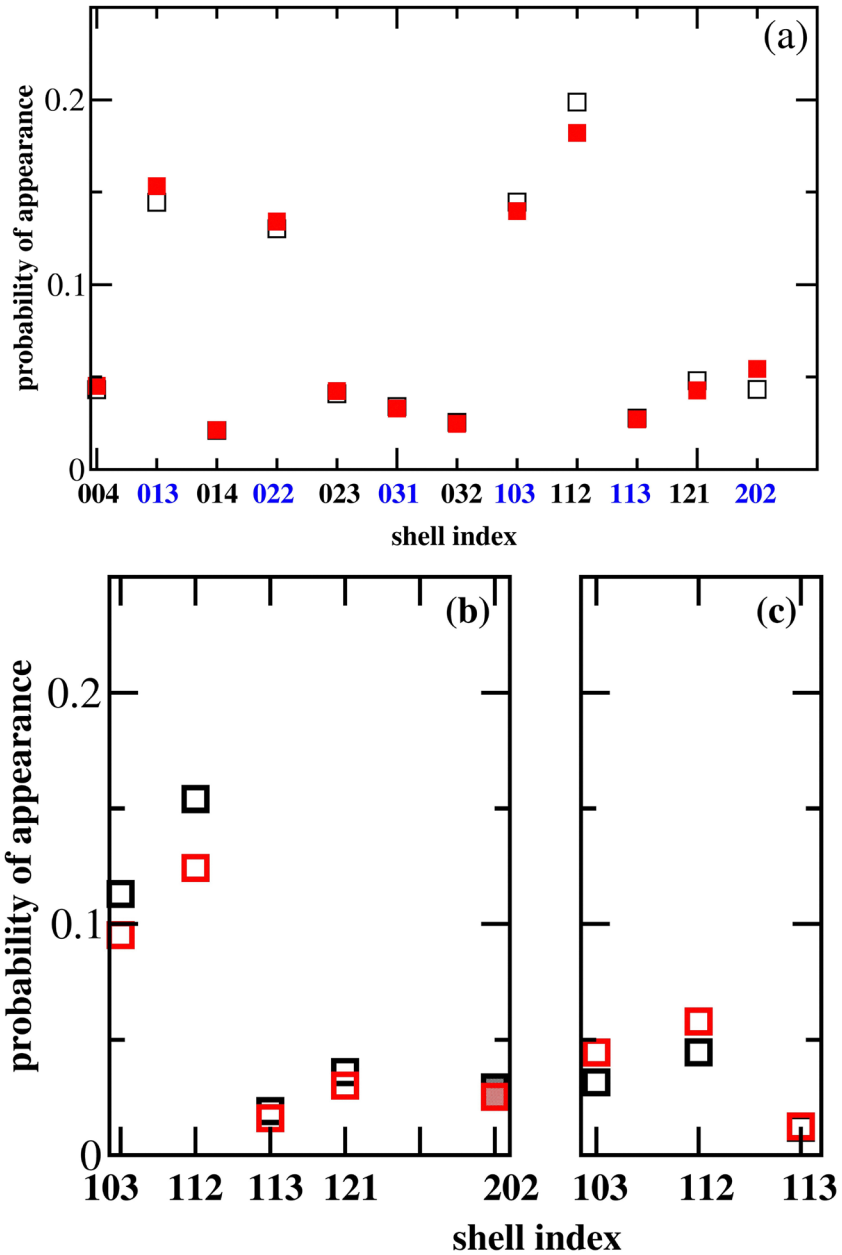


Fig. 3 (a) Probability of Li ion shells (see text for definition of the shell) where anions are not distinguished in the blended salt. For the single salt case the average value of the $PF_6^-$ and the $FSI^-$ electrolyte are plotted. (b) and (c) Probability of Li ion shells, containing one anion or two (like) anions. In contrast to (a) the identity of the anion is taken into account. (b) Contains the case of $PF_6$, (c) the case of FSI. The blended salt data are indicated by black, the single salt data by red symbols. For the incorporation of statistical factors, required for the translation of the probabilities of single salt to the probabilities of blended salt electrolytes in (b) and (c), we have chosen a factor of 2 for the shell, including one anion, and a factor of 4 for the 202 shell, containing two anions. The factors are explained in the main text. We have taken into account Li ion shells with probabilities (in the blended salt electrolyte) of at least 1/52, corresponding to one shell per system.

This analysis was repeated for a salt concentration of 2 M. Here we clearly see stronger deviations from random mixing, governed by more complex interaction patterns.

Summarizing the structural analysis, the blended salt electrolyte can be described in good approximation as a random mixture of the two types of anions. The remaining deviations from a random mixture can be related to the stronger Li–$PF_6$ interaction as compared to the Li–FSI interaction.

### 3.2 Ionic conductivity and diffusivity

The single salt $LiPF_6$ electrolyte system has been studied in detail in ref. 24. Its ionic conductivity at 0.95 M is again shown in Fig. 4. The experimental value shown in the plot is higher than the simulation value due to the slightly different EC : EMC solvent ratio. The previous work[24] reported that the ionic conductivity increases with increasing EC : EMC solvent ratio, so a lower value is expected for EC : EMC 24 : 76, the solvent

 

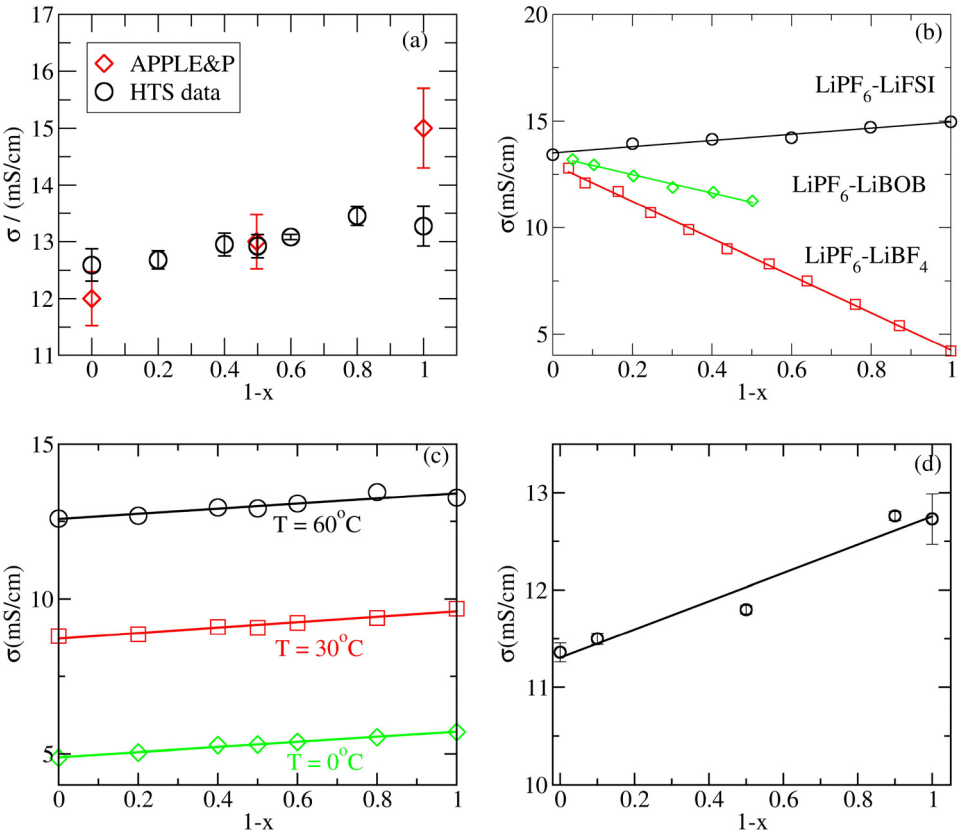


Fig. 4 (a) Ionic conductivity $\sigma$ *vs.* $(1 - x)$, where mol fraction of LiFSI $x = N(\text{LiFSI})/(N(\text{LiPF}_6) + N(\text{LiFSI}))$, with $x = 0$ for single salt $\text{LiPF}_6$ electrolyte and $x = 1$ for single salt LiFSI electrolyte. The blended salt electrolyte corresponds to $x = 0.5$. The experimental data result from high-throughput screening (HTS) experiments. (b) Experimental conductivity *vs.* $1 - x$ for three salt mixtures shown by symbols with a linear fit. The simulations and measurements, shown in this figure, have been performed at 333 K. (c) The experimental ionic conductivity *vs.* $1 - x$ for $\text{LiPF}_6$–LiFSI mixtures. (d) Experimental data of ionic conductivity *vs.* $1 - x$ for the salt concentration 2 M and temperature 333 K of $\text{LiPF}_6$–LiFSI mixtures.

ratio used in the simulations, than for 30 : 70, the solvent ratio in the experimental system. A rough estimate of the ionic conductivity for the 30 : 70 EC : EMC solvent ratio is made from the plot of ionic conductivity *vs.* EC : EMC solvent ratio in ref. 24, and the extracted value of 13.13 mS $\text{cm}^{-1}$ marked with an asterisk in the plot Fig. 4 is in excellent agreement with the experiment. In agreement with the experiment we also see an approximately linear increase of the ionic conductivity upon substituting $\text{PF}_6$ by FSI which, within the statistical uncertainties is compatible with the experimentally observed dependence. In conclusion, the agreement of the simulated ionic conductivities with the experimental results is promising so that the results of the simulations may be taken as a basis for a closer microscopic analysis.

To establish that linear interpolation in a salt blend is a universal phenomenon, we fit the experimental data of the ionic conductivity $\sigma$ of three salt blends, shown in Fig. 4(b), linearly with respect to the LiFSI mole fraction. Indeed, a very good agreement with the experimental data is observed.

Next, we have checked whether the linear interpolation of the conductivity also holds for other temperatures. Therefore, we present additional data also for 0 °C (273 K) and 30 °C (303 K) for the $\text{LiPF}_6$–LiFSI case. As shown in Fig. 4(c), for all temperatures the data are consistent with a strictly linear behavior. Finally, we have checked whether this linearity still holds for the higher salt concentration 2 M. Interestingly, now significant deviations occur, see Fig. 4(d). This is consistent with the much stronger deviations from random mixing at this high salt concentration.

Furthermore, we have extracted the individual diffusion constants and the resulting N–E conductivity for the different systems. They are listed in Table 1. It turns out that within 5% the diffusion constants of the two anions in the blended salt are the same as in the respective single salt electrolytes. This is a first indication that not only the structural but also the

Table 1 Diffusion coefficient and N–E conductivity

| Formulation | Ion | Diffusion coefficient $D/(10^{-10}\ \text{m}^2\ \text{s}^{-1})$ | N–E conductivity $\sigma_{\text{NE}}/(\text{mS cm}^{-1})$ |
|---|---|---|---|
| $\text{LiPF}_6$ single salt | $\text{Li}^+$ | 4.3 ± 0.01 | 29.3 ± 0.2 |
| | $\text{PF}_6^-$ | 5.1 ± 0.02 | |
| LiFSI/$\text{LiPF}_6$ blended salt | $\text{Li}^+$ | 4.2 ± 0.01 | 29.1 ± 0.1 |
| | $\text{PF}_6^-$ | 4.8 ± 0.016 | |
| | $\text{FSI}^-$ | 5.8 ± 0.02 | |
| LiFSI single salt | $\text{Li}^+$ | 4.0 ± 0.01 | 29.1 ± 0.1 |
| | $\text{FSI}^-$ | 5.5 ± 0.012 | |

dynamical properties display mixing invariance. In another remarkable observation we see that the N–E conductivity is approximately constant. Thus, the significant differences between the conductivities of the two single salt systems have to do with the cross correlations among different ions which are not included in the N–E conductivity. In particular, the dependence of the conductivity on the salt content has to be determined by the corresponding dependence of the cross correlation terms. Furthermore, since the ionic conductivity is approximately reduced by a factor of 2 as compared to the N–E conductivities, the contributions of the cross correlations need to be large.

As already observed in ref. 24 and 30, N–E conductivities and viscosities follow the Stokes–Einstein relation for a given EC : EMC solvent ratio. Thus, we would expect the viscosities for the three cases should be the same, in agreement with our observations, as shown in the ESI.†

### 3.3 Coupling of contact ion pairs

A major contribution to cross correlations are the dynamic properties of contact ion pairs. We first study the distribution of $\Delta v_{\parallel}$. The results are shown in Fig. 5 for $t$ = 225 ps. During this time the lithium ions have approximately travelled a distance of 7 Å which is more than twice the equilibrium distance between lithium and the two anionic species. The distribution can be described as a Gaussian, characterized by its first moment $\mu$ and its variance $\sigma^2$, together with a superimposed wing on the left side. Thus, for a quantitative analysis we fit the distribution by a Gaussian by minimizing the deviations from the right wing and the region close to the maximum. Along with this Gaussian fit one gets information about the fraction of contacts, which contribute to the Gaussian. The fraction of pairs, contributing to the Gaussian is denoted $cv$. Thus, $(1 - cv)$ may be interpreted as the number of anions which have disengaged from their initial contact cation. For stronger effective coupling between the anion and the cation one may expect small absolute values of $\mu$, $\sigma$, and $(1 - cv)$. Finally, we mention that in analogy to previous work[25] the anions, contributing to the Gaussian, need not necessarily form a contact pair anymore. The reason is that due to hydrodynamic effects also anions in the second coordination shell may also flow together with the tagged lithium ion.

Table 2 Li-anion $\lambda(t)$ values

| $t$/ps | $FSI^-$ single | $FSI^-$ blended | $PF_6^-$ blended | $PF_6^-$ single |
|---|---|---|---|---|
| 75 | 0.626 ± 0.002 | 0.638 ± 0.009 | 0.776 ± 0.007 | 0.778 ± 0.008 |
| 225 | 0.55 ± 0.008 | 0.56 ± 0.02 | 0.75 ± 0.01 | 0.76 ± 0.01 |
| 750 | 0.36 ± 0.01 | 0.33 ± 0.04 | 0.62 ± 0.01 | 0.64 ± 0.01 |

As a key result, we see that the whole distribution of $\Delta v_{\parallel}$ is basically identical for the single salt and the blended salt electrolytes. This clearly shows that not only the structural properties but also the dynamic properties of contact ion pairs display mixing invariance. From the fitting we obtain $|\mu(PF_6)| < |\mu(FSI)|$, $\sigma(PF_6) < \sigma(FSI)$, and $cv(PF6) > cv(FSI)$. There results are consistent with the stronger binding of the lithium ions to $PF_6$. This establishes a second relation between structural and dynamical data.

To obtain information on the time dependence one can study the coupling constant $\lambda(t)$. In Table 2 we tabulate $\lambda(t)$ for single salt and blended salt electrolyte formulations at three

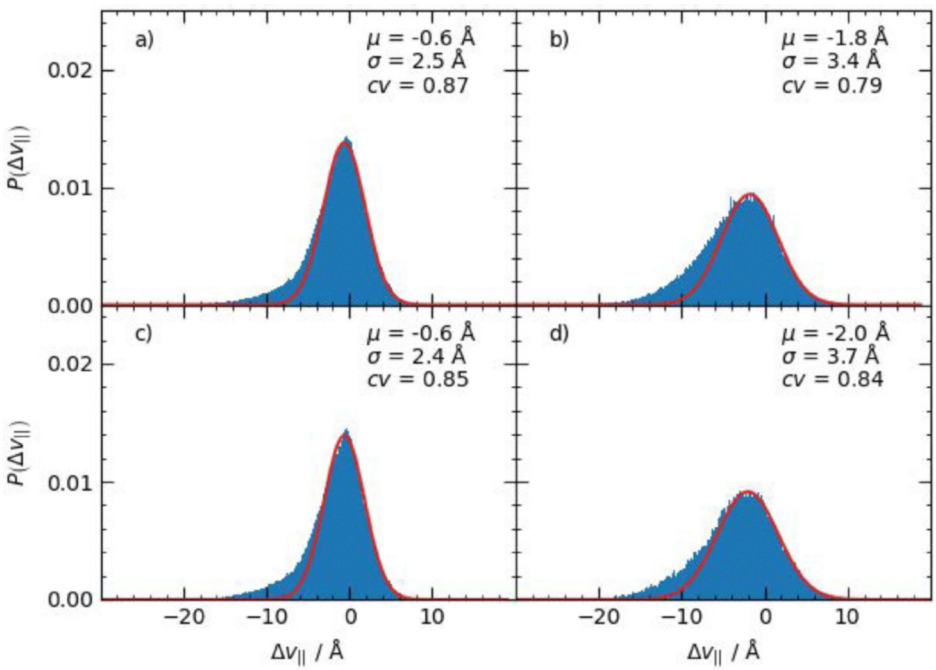


Fig. 5 Transport behaviour of (a) Li–$PF_6$ from the single salt electrolyte formulation, (b) Li–FSI from the single salt electrolyte formulation, (c) Li–$PF_6$ in the blended salt electrolyte, and (d) Li–FSI in the blended salt. The distribution of $v_{\parallel}$ has mean, standard deviation and fraction of contacts denoted as $\mu$, $\sigma$, and $cv$. The data have been obtained for $t$ = 225 ps.

 

Table 3 Cross correlations extracted at a lag time of 1000 ps

| Formulation | ++/NE | +−/NE | −−/NE |
|---|---|---|---|
| $LiPF_6$ single salt | −0.15 ± 0.01 | 0.18 ± 0.02 | −0.07 ± 0.02 |
| LiFSI/$LiPF_6$ blended salt | −0.16 ± 0.01 | 0.13 ± 0.01 | −0.14 ± 0.03 |
| LiFSI single salt | −0.14 ± 0.01 | 0.09 ± 0.02 | −0.16 ± 0.02 |

different times. As expected, $\lambda(t)$ decreases with time, reflecting the slow disintegration of contact ion pairs. $\lambda(t)$ is higher for single salt $LiPF_6$ than for single salt LiFSI electrolytes, consistent with the analysis above of the complete distribution. In particular, the mixing invariance is showing up again. Furthermore, one can see that for $LiPF_6$ pairs the separation of cation and anion takes much longer than for LiFSI pairs which again highlights the impact of different interaction strengths.

### 3.4 Cross correlations

The cross correlations $\sigma_{++}$, $\sigma_{--}$, and $\sigma_{+-}$, normalized by the N–E conductivity $\sigma_{NE}$, are listed in Table 3. Whereas $\sigma_{++}/\sigma_{NE}$ does not change much, both $\sigma_{--}/\sigma_{NE}$ and $\sigma_{+-}/\sigma_{NE}$ show a considerable dependence on the salt composition. Interestingly, the value of $\sigma_{+-}/\sigma_{NE}$ for the blended salt electrolytes results from linear interpolation of the values for the two single salt electrolytes, whereas the value of $\sigma_{--}/\sigma_{NE}$ for the blended salt electrolyte is closer to that of the single salt Li–FSI electrolyte. Although the deviations from linear interpolation (−0.137 *vs.* −0.112) may still be explained by statistical uncertainties, general arguments for this tendency are given below. Since $\sigma_{NE}$ is basically constant, this (approximate) linear interpolation is the underlying reason for the (approximate) linear behavior of the overall conductivity, as already shown in Fig. 4.

Both the degree of random mixing and mixing invariance influence the cross correlations. Since random mixing is fulfilled to a very good approximation, we need to better understand the dynamic properties of tagged cation–cation, cation–anion, and anion–anion pairs. For this purpose, we have calculated the cross correlations in dependence on the distance of the respective pairs, determined from the configurations at the beginning of the considered time interval. The appropriately normalized results are shown in Fig. 6(a)–(d). The results for the blended salt electrolyte formulation agree well with those of the two single salt electrolyte formulations for all distances, except for a slight deviation for LiFSI. Whereas the short range regime is specific for each pair, the long range decay due to hydrodynamic interactions is very similar for the different cross correlations and reaches negative values for even

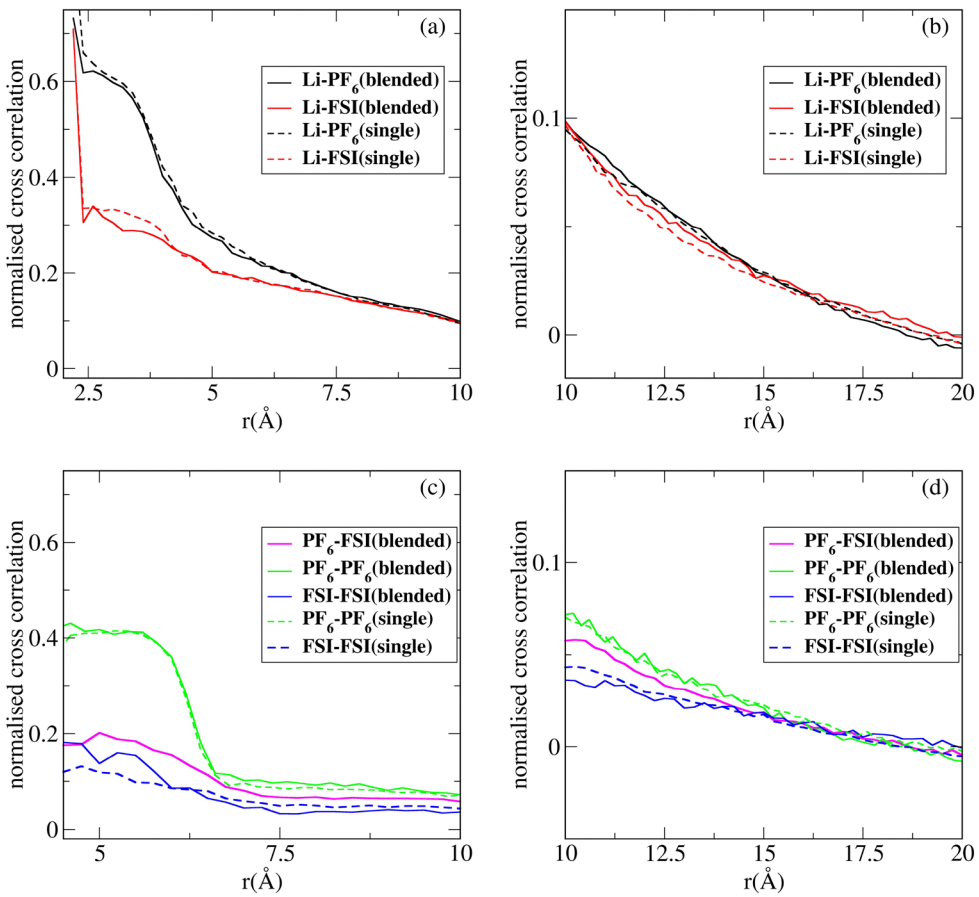


Fig. 6 Cross correlations (a) and (b) $\sigma_{+-}$, and (c) and (d) $\sigma_{--}$ comparison between blended salt and single salt electrolyte formulations. The cross correlations are normalized by the square root of the geometric mean of the mean squared displacements of the involved constituents (lithium–lithium, lithium anion, or anion–anion, respectively).

larger distances. An analytical expression for this decay has been given in ref. 31. Note that the short range correlation of nearby cation pairs and anion pairs is positive despite the repulsive Coulomb interaction. This is related to the cooperative dynamics of local clusters, involving positively and negatively charged ions, as well as neutral molecules.[31]

It is expected that a strong coupling of pairs increases the degree of cross-correlation of nearby molecules. This is the case for $LiPF_6$, showing the strongest interaction and, consequently, the largest short-distance contribution to $\sigma_{+-}$. This translates into $\sigma_{+-}$ ($LiPF_6$) > $\sigma_{+-}$ (LiFSI). The situation is more complicated for the anion–anion pairs. Again, the effective attractive interaction of nearby $PF_6$–$PF_6$ pairs as compared to the lack of attraction of FSI–FSI pairs translates into a higher positive correlation for short distances. However, the universal negative contribution at long distances, as introduced above, finally gives rise to an overall negative value of $\sigma_{--}$. As a consequence, one has 0 > $\sigma_{--}$ ($PF_6$–$PF_6$) > $\sigma_{--}$ (FSI–FSI), the difference between $PF_6$–$PF_6$ and FSI–FSI resulting from the different contributions at short distances. Furthermore, from Table 3 one can see that $\sigma_{++}/\sigma_{NE}$ is basically identical for all cases and displays a value similar to $\sigma_{--}$(FSI–FSI)/$\sigma_{NE}$. This observation is not surprising, since similarly to FSI–FSI pairs there is a lack of short-range attractive interaction for adjacent lithium ions so that the negative hydrodynamic contribution dominates the overall cross correlation. In summary, the overall ionic conductivity for the two single salt electrolyte formulations differs mainly due to the different contributions of $\sigma_{+-}$ and $\sigma_{--}$. For $LiPF_6$ the impact of a larger $\sigma_{+-}$, contributing to a reduction in ionic conductivity, is partially weakened due to the larger value of $\sigma_{--}$. Both effects are a consequence of the stronger $PF_6$–$PF_6$ interaction of nearby pairs.

Finally, as seen in Fig. 6(c) the $PF_6$–FSI short-range correlations are similar to the FSI–FSI pairs. This is not surprising since both pairs display a similar RDF. As a consequence, $\sigma_{--}/\sigma_{NE}$ for the blended salt electrolyte should not be a simple interpolation of the two limiting cases but closer to the value of the single salt LiFSI electrolyte as already mentioned in the discussion of Table 2.

## 4 Conclusion

Experimentally, we have shown that the ionic conductivity for three different blended salt electrolytes linearly interpolates between the values, observed for the limiting single salt electrolytes. For the specific case of the conducting salts $LiPF_6$ and LiFSI a microscopic understanding of the dependence of the ionic conductivity on the anion composition has been developed. For this purpose we have analysed to which degree the properties of nearby Li–$PF_6$ and Li–FSI pairs are changing when comparing the blended salt electrolytes with the respective single salt for an overall salt concentration of 0.95 M. First, it turns out that to a very good approximation mixing invariance is present for many observables. Structurally, the properties of lithium anion pairs remain the same when comparing blended salt and single salt electrolytes. Furthermore, a much stronger coupling of Li ions with $PF_6$ as compared to FSI is observed which gives rise to slight corrections to random mixing *via* a slightly increased number of Li–$PF_6$ and a slightly reduced number of Li–FSI pairs. This can be rationalized by the presence of a thermodynamic driving force in the blended salt electrolyte to form Li–$PF_6$ pairs. However, we have also seen that there is no spatial separation of both anions so that in general random mixing is fulfilled quite well. The structural mixing invariance directly translates into analogous properties for dynamic observables (diffusivity, ionic cross correlations $\sigma_{+-}$ and coupling of contact pairs). The situation is slightly more complex for $\sigma_{++}$ and $\sigma_{--}$. However, as discussed the deviations from mixing invariance are small. This rationalizes the approximately linear dependence of conductivity on salt composition. Due to the generality of the present results, one may expect that also other mixtures of conducting salts display random mixing and mixing invariance. However, different aspects may complicate the situation such as a very different interaction strength of the two anions with lithium or a strong clustering tendency of one of the two salts. And please note that the present results werde obtained for a restricted temperature regime between 273 K and 333 K.

For blended salt electrolytes that exhibit linear superposition, the optimization of the electrolyte formulation may focus on other electrochemical properties that are strongly related to the interaction between the electrolyte and the electrode. Here, additional non-trivial mechanisms may become relevant, which may lead to the main challenge in designing the electrolyte composition by mixing.

## Conflicts of interest

There are no conflicts to declare.

## Data availability

The trajectory files, used for the present analysis, together with a brief explanation have been uploaded to zenodo and can be found on **https://doi.org/10.5281/zenodo.14856280**.

## Acknowledgements

The authors acknowledge funding from the European Unions Horizon 2020 research and innovation program under Grant Agreement No. 957189 (BIG-MAP) and 957213 (BATTERY2030PLUS). Helpful discussions with Youssef Mabrouk are acknowledged.

## References

1 K. Xu, Nonaqueous Liquid Electrolytes for Lithium-Based Rechargeable Batteries, *Chem. Rev.*, 2004, **104**, 4303–4417.
2 K. Xu, Electrolytes and Interphases in Li ion Batteries and Beyond, *Chem. Rev.*, 2014, **114**, 11503–11618.
3 D. Deng, Li ion batteries: basics, progress, and challenges, *Energy Sci. Eng.*, 2015, **3**, 385–418.

 

4 R. Younesi, G. M. Veith, P. Johansson, K. Edström and T. Vegge, Lithium salts for advanced lithium batteries: Li–metal, Li–$O_2$, and Li–S, *Energy Environ. Sci.*, 2015, **8**(7), 1905–1922.
5 Y.-K. Liu, C.-Z. Zhao, J. Du, X.-Q. Zhang, A.-B. Chen and Q. Zhang, Research Progresses of Liquid Electrolytes in Lithium-Ion Batteries, *Small*, 2023, **19**, 2205315.
6 E. Krämer, T. Schedlbauer, B. Hoffmann, L. Terborg, S. Nowak, H. J. Gores, S. Passerini and M. Winter, Mechanism of Anodic Dissolution of the Aluminum Current Collector in 1 M LiTFSI EC : DEC 3 : 7 in Rechargeable Lithium Batteries, *J. Electrochem. Soc.*, 2012, **160**, A356.
7 C. L. Berhaut, D. Lemordant, P. Porion, L. Timperman, G. Schmidt and M. Anouti, Ionic association analysis of LiTDI, LiFSI and $LiPF_6$ in EC/DMC for better Li ion battery performance, *RSC Adv.*, 2019, **9**, 4599–4608.
8 L. D. Ellis, J. Xia, A. J. Louli and J. R. Dahn, Effect of Substituting $LiBF_4$ for $LiPF_6$ in High Voltage Lithium-Ion Cells Containing Electrolyte Additives, *J. Electrochem. Soc.*, 2016, **163**, A1686.
9 K. Xu, S. S. Zhang, U. Lee, J. J. Allen and T. R. Jow, LiBOB: is it an alternative salt for lithium ion chemistry?, *J. Power Sources*, 2005, **146**, 79–85.
10 X. Zhang and T. M. Devine, Passivation of Aluminum in Lithium-Ion Battery Electrolytes with LiBOB, *J. Electrochem. Soc.*, 2006, **153**, B365–B369.
11 M. S. Ding and T. R. Jow, How Conductivities and Viscosities of PC-DEC and PC-EC Solutions of $LiBF_4$, $LiPF_6$, LiBOB, $Et_4NBF_4$, and $Et_4NPF_6$ Differ and Why, *J. Electrochem. Soc.*, 2004, **151**, A2007–A2015.
12 A. Benayad, D. Diddens, A. Heuer, A. N. Krishnamoorthy, M. Maiti, F. L. Cras, M. Legallais, F. Rahmanian, Y. Shin and H. Stein, *et al.*, High-throughput experimentation and computational freeway lanes for accelerated battery electrolyte and interface development research, *Adv. Energy Mater.*, 2022, **12**, 2102678.
13 S. S. Zhang, An unique lithium salt for the improved electrolyte of Li ion battery, *Electrochem. Commun.*, 2006, **8**, 1423–1428.
14 G. Xu, X. Shangguan, S. Dong, X. Zhou and G. Cui, Formulation of Blended-Lithium-Salt Electrolytes for Lithium Batteries, *Angew. Chem.*, 2020, **59**(9), 3400–3415.
15 L. D. Ellis, I. G. Hill, K. L. Gering and J. R. Dahn, Synergistic Effect of $LiPF_6$ and $LiBF_4$ as Electrolyte Salts in Lithium-Ion Cells, *J. Electrochem. Soc.*, 2017, **164**, A2426–A2433.
16 C. Wang, L. Yu, W. Fan, J. Liu, L. Ouyang, L. Yang and M. Zhu, Lithium Difluorophosphate As a Promising Electrolyte Lithium Additive for High-Voltage Lithium-Ion Batteries, *ACS Appl. Energy Mater.*, 2018, **1**, 2647–2656.
17 Y. Li, B. Cheng, F. Jiao and K. Wu, The Roles and Working Mechanism of Salt-Type Additives on the Performance of High-Voltage Lithium-Ion Batteries, *ACS Appl. Mater. Interfaces*, 2020, **12**, 16298–16307.
18 L. Li, W. Lv, J. Chen, C. Zhu, S. Dmytro, Q. Zhang and S. Zhong, Lithium Difluorophosphate ($LiPO_2F_2$): An Electrolyte Additive to Help Boost Low-Temperature Behaviors for Lithium-Ion Batteries, *ACS Appl. Energy Mater.*, 2022, **5**, 11900–11914.
19 A. Mistry, Z. Yu, B. L. Peters, C. Fang, R. Wang, L. A. Curtiss, N. P. Balsara, L. Cheng and V. Srinivasan, Toward Bottom-Up Understanding of Transport in Concentrated Battery Electrolytes, *ACS Cent. Sci.*, 2022, **8**, 880–890.
20 S. Dajnowicz, G. Agarwal, J. M. Stevenson, L. D. Jacobson, F. Ramezanghorbani, K. Leswing, R. A. Friesner, M. D. Halls and R. Abel, High-Dimensional Neural Network Potential for Liquid Electrolyte Simulations, *J. Phys. Chem. B*, 2022, **126**, 6271–6280.
21 I.-B. Magdau, D. J. Arismendi-Arrieta, H. E. Smith, C. P. Grey, K. Hermansson and G. Csányi, Machine Learning Force Field for Molecular Liquids: EC/EMC Binary Solvent, *npj Comput. Mater.*, 2023, **9**, 146.
22 O. Borodin, Polarizable force field development and molecular dynamics simulations of ionic liquids, *J. Phys. Chem. B*, 2009, **113**, 11463–11487.
23 D. Bedrov, J. P. Piquemal, O. Borodin, A. D. MackerrelJr, B. Roux and C. Schroeder, Molecular Dynamics Simulations of Ionic Liquids and Electrolytes Using Polarizable Force Field, *Chem. Rev.*, 2019, **119**, 7940–7995.
24 M. Maiti, A. N. Krishnamoorthy, Y. Mabrouk, N. Mozhzhukhina, A. Matic, D. Diddens and A. Heuer, Mechanistic understanding of the correlation between structure and dynamics of liquid carbonate electrolytes: impact of polarization, *Phys. Chem. Chem. Phys.*, 2023, **25**, 20350–20364.
25 A. Wettstein, D. Diddens and A. Heuer, Controlling $Li^+$ transport in ionic liquid electrolytes through salt content and anion asymmetry: a mechanistic understanding gained from molecular dynamics simulations, *Phys. Chem. Chem. Phys.*, 2022, **24**, 6072–6086.
26 H. C. Andersen, Rattle: A "Velocity" Version of the Shake Algorithm for Molecular Dynamics Calculations, *J. Comput. Phys.*, 1983, **51**, 24–34.
27 G. J. Martyna, T. M. E. Tuckerman, D. J. Tobias and M. L. Klein, Explicit reversible integrators for extended systems dynamics, *Mol. Phys.*, 1996, **87**(5), 1117–1157.
28 L. Lagardere, F. Avait and J. P. Piquemal, Pushing the Limits of Multiple-Time-Step Strategies for Polarizable Point Dipole Molecular Dynamics, *J. Phys. Chem. Lett.*, 2019, **10**, 2593–2599.
29 N. Chapman, O. Borodin, T. Yoon, C. C. Nguyen and L. B. Lucht, Spectroscopic and density functional theory characterization of common lithium salt solvates in carbonate electrolytes for lithium batteries, *J. Phys. Chem. C*, 2017, **121**(4), 2135–2148.
30 A. N. Krishnamoorthy, C. Wölke, D. Diddens, M. Maiti, Y. Mabrouk, P. Yan, M. Günebaum, M. Winter, A. Heuer and I. Cekic-Laskovic, Data-Driven Analysis of High-Throughput Experiments on Liquid Battery Electrolyte Formulations: Unraveling the Impact of Composition on Conductivity, *Chem. Methods*, 2022, **2**, e202200008.
31 D. Diddens and A. Heuer, Hydrodynamic interactions in ion transport—Theory and simulation, *J. Chem. Phys.*, 2023, **158**, 154112.